Running head: High-resolution isotope analysis of tree rings

Progress in high-resolution isotope-ratio analysis of tree rings using laser ablation

Matthias Saurer[1], Elina Sahlstedt[2], Katja T. Rinne-Garmston[2], Marco M. Lehmann[1], Manuela Oettli[1], Arthur Gessler[1,3], Kerstin Treydte[1]

[1]Swiss Federal Institute for Forest, Snow and Landscape Research WSL, Zürcherstrasse 111, 8903 Birmensdorf, Switzerland

[2]Natural Resources Institute Finland (Luke), Latokartanonkaari 9, 00790 Helsinki, Finland

[3]Institute of Terrestrial Ecosystems, ETH Zurich, Universitaetstrasse 16, 8092 Zurich, Switzerland

Corresponding author: Matthias Saurer, matthias.saurer@wsl.ch

For submission to: Tree Physiology, as Methods paper

Keywords

Stable isotopes, climate reconstruction, method development, laser analysis

Abstract

Stable isotope ratio analysis of tree rings has been widely and successfully applied in recent decades for climatic and environmental reconstructions. These studies were mostly conducted at an annual resolution, considering one measurement per tree ring, often focusing on latewood. However, much more information could be retrieved with high-resolution intra-annual isotope studies, based on the fact that the wood cells and the corresponding organic matter are continuously laid down during the growing season. Such studies are still relatively rare, but have a unique potential for reconstructing seasonal climate variations or short-term changes in physiological plant properties, like water-use efficiency. The reason for this research gap is mostly technical, as on the one hand sub-annual, manual splitting of rings is very tedious, while on the other hand automated laser ablation for high-resolution analyses is not yet well established and available. Here, we give an update on the current status of laser ablation research for analysis of the carbon isotope ratio ($\delta^{13}C$) of wood, describe an easy-to-use laser ablation system, its operation and discuss practical issues related to tree core preparation, including cellulose extraction. The results show that routine analysis with up to 100 laser shot-derived $\delta^{13}C$-values daily and good precision and accuracy (ca. 0.1‰) comparable to conventional combustion in an elemental analyser are possible. Measurements on resin-extracted wood is recommended as most efficient, but laser ablation is also possible on cellulose extracted wood pieces. Considering the straightforward sample preparation, the technique is therefore ripe for wide-spread application. With this work, we hope to stimulate future progress in the promising field of high-resolution environmental reconstruction using laser ablation.

1. Introduction

Stable isotope ratios of tree rings have been used for several decades now as reliable indicators of past climatic, environmental and physiological information (Gessler et al. 2014; McCarroll and Loader 2004). The carbon isotope ratio ($\delta^{13}C$) of leaf assimilates is directly impacted by climatic variables that influence stomatal conductance and photosynthetic assimilation rate (see Farquhar et al. (1989) for the theory of photosynthetic carbon isotope discrimination). These variables are mainly soil moisture, vapor-pressure deficit (VPD), temperature and light, whereby the relative importance depends on the climatic zone and local site conditions. Accordingly, various studies have successfully reconstructed climate variables over many centuries, recently even for more than two millennia (e.g. Büntgen et al. (2021); Nakatsuka et al. (2020)), and have established past spatial hydro-climatic patterns (Leavitt and Long 1988; Treydte et al. 2007). Most of these studies have a temporal resolution of one year. This means that tree cores are either separated at their annual borders or only the latewood (LW) portion is cut out, the part of the ring which is considered to best reflect the current year's climatic conditions, although the boundary between earlywood (EW) and LW cannot always be objectively determined. The cells of an individual tree ring are built successively over a growing season, and the phenology and seasonal dynamics influence the involved processes, such as cell enlargement and cell wall thickening (Cuny et al. 2014)..

Various studies have made use of the more hidden high-resolution (intra-annual) information by measuring tree-ring isotope ratios by laser ablation (Skomarkova et al. 2006) or on manually cut micro sections (Kagawa et al. 2006; Martìnez-Sancho et al. 2022; Nabeshima et al. 2018). Examples for the value of high-resolution isotope studies are from the tropics, where clear visible annual patterns are mostly lacking, but cyclic isotope patterns have sometimes been found (Schollaen et al. 2014; Verheyden et al. 2004). In deciduous species, the EW part of rings has been found to have relatively high $\delta^{13}C$, due to the use of ^{13}C-enriched starch for cell formation, reflecting remobilization of assimilates stored in previous years (Hafner et al. 2015; Helle and Schleser 2004). A general tri-phase pattern in deciduous species over the course of a ring has been discovered, which is characterized by high values for the first EW cells followed by a decrease and a minimum in the first part of the LW and a steep increase towards the end of the ring (Helle and Schleser 2004). These results raised concerns about a strong impact of post-photosynthetic biochemical fractionation factors on the intra-ring $\delta^{13}C$ patterns, potentially disturbing and diminishing climatic information.

In evergreen pine trees, however, EW production strongly depends on current-year photosynthates (Barbour et al. 2002; Dickmann and Kozlowski 1970) and therefore intra-ring isotope patterns in evergreen species may better reflect actual climate than in deciduous species (Monson et al. 2018). Indeed, studies of pine species in several regions of the Northern Hemisphere showed the potential to infer seasonal climate information from $\delta^{13}C$ intra-ring patterns (Kagawa et al. 2006; Ogée et al. 2009). Moreover, comparison of $\delta^{13}C$ of biweekly sampled leaf sugars, representative for recent assimilates, and intra-annual tree ring $\delta^{13}C$ showed comparable trends in *Pinus sylvestris* (Offermann et al. 2011). In Siberia, a strong seasonal climate signal was found in a laser ablation study on *Pinus sylvestris* (Fonti et al. 2018), particularly for young trees, while older trees may have been more affected by carry-over effects of the previous year's growing conditions on current year's wood production. In the Mediterranean as well as in the Western US, intra-annual density fluctuations (IADFs) or "false LW" are frequent that show promise for reconstruction of seasonal drought periods. IADFs are visible bands within a ring that can be caused by unusually dry and subsequent wet conditions. They can be understood as hydraulic adjustments by wood anatomical changes to water stress, as observed in *Pinus pinea*, which also impact the isotope ratios in these wood structures (Battipaglia et al. 2010; Zalloni et al. 2018). For *Pinus ponderosa*, the importance of phenological lags for understanding the isotopic signatures of false LW bands was shown, but also the ability to infer seasonal climate signals (Belmecheri et al. 2018). The latter was also shown by analysing EW and LW separately for *Pinus ponderosa* (Szejner et al. 2018). For deciduous members of the *Pinaceae* family, *Larix* species analysed in Siberia showed great promise for high-resolution studies. The seasonal leaf sugar $\delta^{13}C$ patterns in *Larix gmelinii* were well recorded in the intra-annual tree-ring $\delta^{13}C$ pattern, albeit dampened (Rinne et al. 2015). The different seasonal weather conditions of the two investigated years in this laser ablation study showed clearly different tree-ring $\delta^{13}C$ patterns related to the atmospheric vapour pressure deficit. This opens the possibility to reconstruct such high-resolution climatic information over the past.

In view of the great potential of high-resolution isotope analyses, the relative rareness of such studies may be surprising. This lack is most likely related to the tedious amount of preparation necessary for manually cutting thin slices of rings, e.g., using a microtome (Treydte et al. 2014; Verheyden et al. 2004). Laser dissection (Schollaen et al. 2014) and laser ablation combined with isotope-ratio mass-spectrometry (LA-IRMS) are potentially less cumbersome than manual cutting, but the challenging techniques involve various independent devices and are still not widely applied (Loader et al. 2017; Rinne-Garmston et al. 2022; Schulze et al. 2004). The laser

dissection technique has the advantage of very precise cutting of individual wood structures, e.g., ray parenchyma, but may not be suited for high-throughput analyses, as each cut wood piece is first transferred to an individual silver capsule and later analysed on a different instrument for the isotope ratio (Schollaen et al. 2014). The laser ablation, in principle, enables the integration of all processes from selecting a series of spots on a sample to isotope measurement. Such techniques have been developed and applied also in other research fields (Moran et al. 2011; van Roij et al. 2017; Zhang et al. 2020). However, a dedicated and straight-forward method for tree rings was still lacking until recently.

Here, we describe an LA-IRMS that integrates the complete chain of processes from UV-laser ablation to isotope analysis, including a sample chamber with a large window, high-precision positioning of this chamber, software for placing the desired laser shots, a combustion oven for the ablated dust particles, a CO_2-collecting system and an interface to the IRMS. The integration of all components enables fast and unattended high-throughput analyses, once the laser shots are set. This opens the possibility for systematic assessment of high-resolution analysis. Few papers have described the LA-IRMS method for tree rings in detail so far, mostly referring to the pioneering work from Wieser and Brand (1999) and Schulze et al. (2004). Due to the limited available information, we are convinced that a detailed explanation of the technique is crucial for stimulating its further use and application. In this paper, we therefore provide 1) a description of an LA-IRMS system dedicated to high-resolution tree-ring analysis, its performance and operation; and 2) a discussion of optimal tree-ring sample preparation for this technique, including the option to apply the technique on cellulose.

2. Materials and Methods

2.1 Set-up

The complete LA-IRMS set-up consists of a UV-laser (Teledyne LSX-213 G2+, Nd:YAG Laser; wavelength 213 nm), a sample chamber (isoScell, Terra Analitic, Alba Iulia, Romania), a combustion oven, a Cryoflex trace gas system (Sercon, Crewe, UK) for collection of produced CO_2 with liquid nitrogen (LN_2) traps, a GC-column, an IRMS to measure $\delta^{13}C$ (HS2022, Sercon, Crewe, UK), and controlling software (Fig. 1). An almost identical set-up is installed at WSL, Switzerland, and at Luke, Finland. Here, we present results from both institutes, mentioning differences where applicable.

134 The laser shoots on a sample, normally a piece of wood, through a glass window made of fused
135 silica. The sample can be of maximum length of 4 cm and is placed in a sealed chamber together
136 with reference materials (Fig. 2). The wood sample may need to equilibrate for 1-2 hours in the
137 chamber, as a minor shrinking of the wood core is possible in the completely dry helium stream.
138 The sample chamber is attached to a 3D moving table, which allows precise positioning and
139 movement of the sample (motion control 100 x 100 mm XY travel, 0.16 µm resolution, 50 mm
140 Z travel, 0.78 µm resolution). A video microscope system comprising continuously variable
141 zoom magnification optics is combined with a high-definition color camera capable of resolving
142 sample features down to 2 µm. The microscope is placed perpendicular to the sample and co-
143 axial with the laser beam for distortion-free imaging and ablations. A long sequence of laser
144 shots can be pre-programmed and then run automatically. For the settings, operation and
145 positioning of the laser shots, the laser has its own PC and software, which is connected to the
146 PC of the IRMS by a trigger signal for coordinated operation. The spot size in principle ranges
147 from 4 µm to 200 µm (but see below for more details on applicable range). The laser settings
148 normally used at WSL and Luke are fluence 4 J/cm2, laser output 22.5%, 20 Hz, and 8 J/cm2,
149 laser output 40%, 20 Hz, respectively. The influence of different laser energy is discussed
150 below. The laser has a Class 1 enclosure with safety interlocks that prevent exposure to UV
151 laser light for the operators.

152 The resulting gases and/or particles from the laser ablation are transported with helium (WSL:
153 30 ml/min; Luke: 50 ml/min) through a stainless-steel tubing (outer diameter 1/16 in.; inner
154 diameter: 0.04 in.) to an oven for complete oxidation of all carbon to CO_2 (Silicon Carbide tube
155 furnace model TSH15/16/125). The temperature of the oven is set in the range of 700°C (Luke)
156 to 860°C (WSL) and contains a silica tube (length 370 mm; diameter 6 mm OD, 4 mm ID)
157 filled with Cr_2O_3 (at Luke, length 470 mm, otherwise similar). After the sample has passed the
158 reactor and after completion of each analysis, a valve to an oxygen supply is opened for some
159 seconds to keep the reactor fully oxidized (Fig. 1). The produced gas including CO_2 passes a
160 Nafion trap for water removal and is subsequently collected with LN_2, first in the larger volume
161 trap (trap 1, collection mode, Fig. 1).

162 The CO_2 is subsequently released by lifting the trap and collected in the smaller volume trap 2
163 (smaller volume results in a more distinct sample peak later on). The system then switches to
164 analysis mode (low He flow of 3-4 ml/min), the second trap is lifted and the released CO_2 passes
165 through the GC-column (WSL: Rt-Q-Bond column, Restek, 0.53 mm ID, 30 m, 20 µm; Luke:
166 Rtx Bond, 10 m). The temperature of the column is kept between room temperature and 70 °C
167 (shorter residence time for higher temperatures) for separating CO_2 from other possibly

interfering gases (NO, NO_2, N_2O) that may also be trapped with LN_2. All traps and valves (Fig. 1) as well as the GC-column are part of the CryoFlex Trace gas system (Sercon, Crewe, UK), whose timing and operation are controlled by the IRMS software. Finally, the $\delta^{13}C$ of CO_2 is measured in the IRMS. Significant difference between groups of $\delta^{13}C$ data were assessed by an F-test ($p<0.05$). The size of the mass-spectrometer signal (i.e. "peak size") is dependent on spot size and laser settings, and can be expressed as beam area (given as, i.e. integrated amplifier signal over time).

The analysis time for one sample (i.e. laser shot) is ca. 700 secs for the WSL instrument. This time is given from the complete sequence of operation steps needed, but in particular from passage through the GC-column. It is necessary to complete one sample before beginning the next because the CO_2 accumulates in the traps throughout the laser shot. At Luke, the analysis time is only ca. 300 secs due to shorter length of the GC column. Over-night runs may be limited by the amount of LN_2 fitting in the dewar, which is slowly evaporating. We therefore tested the use of an automated LN_2 refiller (Norhof LN_2 Microdosing System #900). This can enhance the operation time, but care needs to be taken to avoid build-up of ice around the LN_2-traps after prolonged use, which eventually can lead to blockage inside the traps.

2.2 Standard and sample materials

Standards

According to the principle of identical treatment of references and samples (Werner and Brand 2001), a reference material close or similar to wood is recommended to be used during laser ablation. However, unlike for bulk analysis with elemental analysers (EAs), where materials are homogenized, this is more difficult in the case of laser ablation. Intact wood is spatially heterogenous with respect to C-isotope composition and can therefore not be used as a reference material in this application. As a surrogate, cellulose may be used, which is commercially available as pads or mats of varying thickness (Blotting pads, cellulose 100%, VWR, 28298-018). The IAEA-C3 cellulose was formerly also provided as a mat but was additionally homogenized and is now provided as powder. The indicated $\delta^{13}C$-value of -24.72‰ should, however, be verified prior to use (WSL: -24.71‰ ± 0.07‰; Luke: -24.61‰ ± 0.13‰), because older batches of this material may have a different isotope ratio. Powdered materials may also be used as reference for laser ablation when compacting them with a tablet press (WSL: Micro-Tec MTB6, Tablet Press, Micro to Nano, Haarlem, Netherlands; Luke: Perkin Elmer IR

Accessory Hydraulic Press, PerkinElmer, Überlingen, Germany). The $\delta^{13}C$ values of these materials can be determined by analysis with EA-IRMS. Standards used in Luke further include: Yucca inhouse standard (EA: -15.46±0.05‰, n=19); powdered wood reference materials USGS-55 (reported as -27.13± 0.02, n=18).

Tree-ring samples

Tree cores of 10 mm diameter were collected in Pfynwald, a mature Scots pine (*Pinus sylvestris*) forest located in the inner-Alpine dry Valais, Switzerland. Trees at this site are strongly impacted by summer drought, and increased tree mortality has been observed at this site in recent years. It is an extensively monitored and investigated site, and additionally features an irrigation treatment that lasted almost 20 years (Bose et al. 2022). Additionally, a ^{13}C-labelling experiment took place on some of the trees in late summer of 2017 (Joseph et al. 2020), which left a marker in different tree tissues including tree rings. This is ideal for studying carry-over effects of carbohydrates to the following year(s) and to determine how much the carry-over depends on growth conditions such as water availability/drought. For this work, the large ^{13}C-variations from year to year due to labelling were also particularly useful for determining the influence of core surface preparation. Due to the drought stress in the area, tree-ring widths were rather narrow for the investigated years 2015-2018 and for the analysed four trees (tree No. 40: 0.26 ± 0.06 mm, No. 237: 0.57 ± 0.31 mm, No. 466: 0.77 ± 0.18 mm, No. 390: 0.72 ± 0.15 mm).

2.3 Sample preparation methods

We compared LA-IRMS results of the tree cores after application of different surface preparation and solvent extraction methods, considering that sample preparation is important for obtaining reliable $\delta^{13}C$ results, and describe here the optimal procedures based on these tests. Cellulose extraction of whole wood core laths was further tested, following the method in Kagawa et al. (2015), for comparison of laser profiles of wood (with and without resin extraction) and cellulose.

Surface preparation

The tree core surface can be prepared either by cutting with a core-microtome (Gärtner and Nievergelt 2010), by sanding or by a combination of both. The increment cores are fixed in the core holder of a core microtome enabling the cutting of flat surfaces over their entire extent. Ideally, the cut surface of the core preserves the structure of the single cells within the annual rings. This procedure results in the cell walls not being frayed and the surface of the entire core to be flat. In contrast, polishing is done with a sequence of different grit sandpapers, starting for instance with 80-grit, followed by 120, 220, 300-grit (microfinishing film, aluminum oxide, 3M). A final polishing with 400-grit is sufficient for most conifers. For hardwoods and especially tropical species, sanding grits up to 1,200 to distinguish the growth-ring boundaries is recommended. Wood dust in the cells could subsequently be washed out using an ultra-sonic bath (here not done). A combination of the methods means that a microtome cut is followed by just a few strokes with a fine-grit sandpaper to minimize dust distribution across cells, but at the same time enhancing the visual contrast of the xylem cells.

Extractions

To remove resins and other soluble compounds, cores were treated with alcohol in a Soxhlet apparatus (Schweingruber et al. 1978). Samples can be boiled in water to remove hydrophilic compounds, such as phenols and tannins, and refluxed in alcohol, benzene, acetone, or toluene to remove lipophilic substances, such as resins or oils (Björklund et al. 2019).

For cellulose extraction, tree cores were cut into 1.5 mm thick plates, i.e. thin wood strips or laths, of near-even thickness using a twin-blade saw as used also for traditional MXD analysis (preparation for radiography) and packed into F57 fibre filter bags (made of polyester and polyethylene with an effective pore size of 25 µm) for subsequent chemical treatment (Ankom Technology, Macedon, NY, USA). A modified Jayme-Wise holocellulose isolation method was used, involving $NaClO_2$ treatment at 60°C and washes with a 5% NaOH solution at 60°C. This was done based on Boettger et al. (2007), modified for larger numbers of samples that allows for the parallel extraction of up to 400 samples (Weigt et al. 2015).

Using the above methods, we prepared Scots pine tree cores from Pfynwald as 1) untreated, surface cut with microtome, 2) solvent-extracted, cut with microtome, 3) solvent-extracted, cut and briefly polished with sandpaper, and 4) after cellulose extraction (Fig. 3).

3. Results

3.1. Standard tests and influence of laser settings

To evaluate the performance of the LA-IRMS, a range of tests with reference cellulose pads was carried out. A typical example of an automated series of measurements with two different cellulose pads is shown in Fig. 4a, using a laser spot size of 100 µm (measured at WSL). The test demonstrated an overall reproducibility of ca. 0.1 ‰ based on the standard deviation as well as comparison to values obtained from EA-IRMS analysis (IAEA = -24.72‰; VWR= -27.53 ± 0.10‰). There was no apparent memory (carry-over from one sample to the next) that would be observed after changing the sample type from IAEA to VWR. A memory effect could for instance be due to residual dust in the chamber from a previous sample. This can be even better tested when using reference materials with larger differences in isotope values using a tablet press, as done in Luke with materials differing more than 10‰ (Yucca inhouse standard, wood reference materials USGS-55). These results also showed no memory effect and agreement to analysis by EA-IRMS within measurement uncertainty.

Depending on the research question and required spatial resolution, different spot sizes may be of interest. Tests of spot sizes of 20 µm, 30 µm, 40 µm, 50 µm, 100 µm, 150 µm on VWR cellulose are shown in Fig. 4 (intermediate sizes are not available for this laser). It was observed that the IRMS signal (expressed as beam area) is strongly dependent on the spot size, as expected, but potentially also influencing the isotope ratio (Figs. 4b, c). However, between 50 µm and 150 µm, representing a range in beam areas from 2.1e-8 to 2.3e-7 As, the IRMS signal is sufficiently large for reproducible analysis. In this range, there is only a small and linear effect on $\delta^{13}C$, which can be corrected for, if necessary. For spot sizes smaller than 50 µm, the precision is reduced by background effects and non-linearity of the IRMS that may result in increased scatter of $\delta^{13}C$ values (Luke) or a systematic deviation from the expected $\delta^{13}C$ value (WSL, Fig. 4b). For these smaller spot sizes, however, it is possible to ablate a so-called “line of spots” with the laser, as e.g. applied in samples shown in Fig. 3. This means that particles and gas from several spots along a line are collected for one isotope measurement. In this case, a sufficient beam size can also be obtained for 30 µm spot size, with a length of the ablated line of ca. 200 µm (Luke: 40µm spot size and track length of 300-350µm). This is crucial for the analysis of narrow rings. For analysis of small wood structures, such as individual cells, it is also possible to ablate various small spots and collect them for one analysis using the LN_2-traps.

The beam area can also be modified through laser settings, like laser power. There is a steady increase of beam area with laser power (Fig. 5). However, different laser settings need to be carefully tested against unwanted side-effects, like charring. Due to the laser energy and resulting heat, the ablated sample can be assumed to contain significant amounts of gaseous

295 species (CO, CO_2) in addition to particles. Earlier studies reported mainly wood dust as a result
296 of laser ablation, but in this case a laser of lower energy with wavelength of 266 nm was used
297 (Moran et al. 2011; Schulze et al. 2004). The minor occurrence of particles was tested by
298 bubbling the outflow of the laser chamber from several laser shots through a tube with water
299 and the liquid subsequently filtered and investigated under a microscope for particles (not
300 found) as well as combusted in an elemental analyser (no carbon above blank detected). The
301 test without combustion oven showed that only minor amount of CO_2 is produced by the laser
302 ablation at laser power 5-80% (Fig. 5, measured at Luke), in the order of 2-3% in comparison
303 to the amount produced with the hot reactor and less than 1e-9 As. Rather, the production of
304 CO during laser ablation is possible and likely, as the ablation occurs in an oxygen free
305 environment, as well as the production of CH_4. The distribution of ablation products between
306 carbon containing gas and particle phases was found to be strongly matrix dependent (Frick and
307 Günther 2012). For matrices with a high O/C ratio such as wood and cellulose acetate, tests
308 performed with a 193 nm laser showed that mostly gaseous C phases or ultrafine particles were
309 formed (Frick and Günther 2012). In any case, all C-containing compounds, whether gaseous
310 or particles, will be converted to CO_2 in the combustion process. We further could not detect
311 any traces of N_2O (m=44) in the IRMS chromatogram. N_2O could interfere with the analysis of
312 CO_2 because of mass overlap. Laser power also influences the resulting depth of laser holes in
313 the wood (typically 2-3 mm), which is an important consideration for sample and standard
314 material thickness.

315

316 **3.2 Comparison of results for different preparation methods**

317 Results from the Pfynwald Scots pine experiment show that the ^{13}C-label supplied to the tree
318 crowns in 2017 was clearly detectable in the tree rings by $\delta^{13}C$ values outside the range of
319 natural abundance (Fig. 6). We found generally more enriched values of samples that were not
320 solvent extracted compared to extracted samples. The analysis of these extracted cores in
321 replication generally showed good agreement between the two runs, although the maximum
322 ^{13}C-signal in 2017 sometimes differed. This is due to the fact that only few LW cells were
323 developed in these very narrow rings (<0.5 mm) at the end of the summer (when labelling was
324 applied). Therefore, the positioning of the laser spots crucially determined how much of the
325 label, applied in a whole tree ^{13}C exposure experiment (Joseph et al. 2020), was found. The
326 labelling distribution among years also markedly differed between trees. In tree No. 40, for
327 instance, the maximum label was not found in late 2017, but rather in the following year 2018.

For better visibility of the tree rings, we applied an additional manual polishing to the extracted cores and analysed them again. The labelling-peak is ideal for testing a possible smearing of signal by this process, as wood dust may be moved across the cores into adjacent cells. However, we did not find significant differences between extracted and later polished cores. This is clearly demonstrated by the analysis of tree No. 466 with exceptionally high $\delta^{13}C$ values in late 2017 of more than 350‰, which nevertheless shows very similar values during the peak, as well as before and after the peak.

As a further comparison among sample pre-treatments, we measured cellulose laths that were extracted from previously analysed wood cores. Our tests showed that despite reduced visibility of the xylem cell structures, laser ablation is also feasible on cellulose extracted from 1.5 mm thick wood laths (Figs. 3, 7). A precise setting of laser spots is, however, hindered, which is a clear disadvantage, particularly in late 2017 when the maximum ^{13}C-label occurred. Also the handling of the brittle cellulose samples gets more difficult. On average, the cellulose was enriched in ^{13}C by 1.24‰ ± 1.12‰ relative to solvent-extracted wood (excluding LW 2017), but this offset varied somewhat between the years or even within one tree ring (2015).

We found that the IRMS intensity, expressed as beam area, showed annual patterns, most likely reflecting the wood density, a finding not previously reported to our knowledge (Fig. 8). For example, for the year 2015 for the pine sample No. 237, 3-4 laser shots were placed in the LW as apparent from the photo (Fig. 3a). Later, there was an increase in the beam area (Fig. 8), potentially even before the first LW cells become visible. It needs to be considered, however, that beam areas depend on laser parameters, like laser energy, and also mass spectrometer sensitivity.

4. Discussion and conclusion

4.1 Laser operation and isotope analysis

The LA-IRMS described here allows daily routine measurements of up to 100 laser shots and subsequent $\delta^{13}C$ measurements on a wood core. The preparation and programming of a sequence of shots is easy and fast, provided that the wood core surface is prepared in a way that shows the tree rings clearly. Alternatively, for wood samples without distinct tree ring borders, as for instance Mediterranean or tropical wood, it is also straightforward to program a regular sequence of shots with constant distance between each spot. The maximum number of measurements feasible per day is mainly limited by the time for one measurement, which is

given by the sequence of all processes, including laser ablation, combustion, collection and release of CO_2, passage through GC-column and IRMS-analysis. This time is to a large degree constrained by the GC-column used, where shorter length results in shorter CO_2 passage time. The GC-column is important, however, for the separation of potentially interfering gases, like N_2O, which would be collected and released with the LN_2 traps together with CO_2 and could hamper the $^{13}C/^{12}C$ determination due to mass overlap (Ghosh and Brand 2004). In our operation conditions, however, no formation of N_2O was observed, probably because of the generally low N-content of wood (<0.5%) and the formation of NO rather than N_2O during laser ablation and combustion.

The accuracy and precision of the $\delta^{13}C$ measurements are comparable to results obtained by conventional combustion in an elemental analyser (ca. 0.1‰). The recommended procedure for referencing isotope values to the international standard (Werner and Brand 2001) can be applied by inserting reference pad materials with differing isotope ratios into the sample chamber. No carry-over effect from one sample to the next was observed. The indicated precision is, however, only attained when sufficient material is ablated. We routinely used spot sizes between 50 to 100 μm or stripes of 30 μm applied in parallel to the tree ring boundary (Fig. 3). This is sufficient for obtaining intra-annual resolution in most samples, but it also limits the size of the structures that can be analysed or the number of analysis possible in narrow rings. When aiming at small wood structures, such as individual cells, resin ducts, fibers, vessels or parenchyma rays, the resolution may be too coarse. Here, potentially UV laser-dissection may have an advantage (Schollaen et al. 2014).

The LA-IRMS system requires little maintenance (e.g. combustion tube holds many months), so that 5*100=500 laser measurements per week are possible. For comparison with traditional analysis, we estimate here the work necessary for 100 isotope results, which can be done with the laser in on day. This would involve manually cutting 100 (thin) wood slices, milling them individually, packing them in tin capsules, followed by analysis in an EA-IRMS. Including the difficulty of cutting thin slices, which can later be traced back to the position in the ring (because the sample is used up), we estimate at least a week of work, or more likely two, for this process. This means that the laser ablation is faster by a factor of 5-10.

Although the number of analyses with the laser and the high sample throughput may look impressive, it should still be considered that because of the high resolution usually applied even a core of 4 cm, the maximum length fitting into the sample chamber, may need more than one day for the analysis. As an example, assuming a core with ring width of 1 mm, where 5 shots

393 are applied per mm result in 200 shots on a piece of 4 cm for 40 tree rings. Accordingly, analysis
394 of long cores or many trees still takes much measurement time, and a careful design for
395 optimizing the scientific output relative to the analysis time is essential. Laser ablation should
396 thus not be considered an easy method to save the labour of cutting slices of rings, but should
397 be tailored to specific questions difficult to answer with conventional methods. The more
398 traditional cutting of rings and analysis by elemental-analyser can also be done complementary
399 to laser-ablation.

400

401 **4.2 Sample preparation**

402 The preparation of wood cores for laser ablation has the goal to provide a clean and well visible
403 surface. Dating of the rings with traditional dendrochronological methods is first done. Ideally,
404 high-resolution images of the tree rings should be taken, which helps in planning and setting
405 the series of shots for laser ablation. Resins may also need to be removed because they are
406 mobile across the tree-ring boundaries and may have more negative $\delta^{13}C$-values compared to
407 other wood constituents (Rissanen et al. 2021). While the analysis of cores including resins
408 therefore may not be desirable in most cases, it is in fact interesting in labelling studies for
409 studying carbon allocation to resins, as this is a defense mechanism against insects and
410 pathogens. It was shown that Scots pine trees weakened by drought allocate less carbon to
411 resins, potentially also weakening the defense against pathogens (Rissanen et al. 2021). We
412 found ^{13}C-enriched values in untreated wood compared to resin-extracted wood in the Scots
413 pine experiment (Fig. 6), which could be expected as trees incorporate fresh assimilates and
414 thus ^{13}C-labelled carbon quickly into resins (Rissanen et al. 2021). The laser ablation of such
415 untreated material is therefore valuable to study such processes, e.g. the amount and distribution
416 of newly produced resins in the stem, in particular as it is possible to analyse the same cores
417 again after solvent extraction.

418 Polishing and sanding of wood samples is often avoided in isotope analysis (Schollaen et al.
419 2017), because of the potential smearing of wood dust between years, filling up the open wood
420 pores. The cleanest method for surface preparation is therefore with a microtome cut (Gärtner
421 and Nievergelt 2010). However, the visibility of cells and tree-ring boundaries is reduced with
422 this method compared to sanding, which can be a problem, for instance in deciduous wood. The
423 laser operator needs to recognize the tree rings, including EW and LW, to be able to set the
424 shots properly (unless a regular laser pattern is set irrespective of any wood structure). We
425 therefore tested if improving visibility of cells by gently polishing cores that were previously

cut with a microtome does not disturb the isotope profiles and found indeed that this is the case. Alternatively, cores can also be washed in an ultrasonic bath after sanding to remove as much dust as possible (Tang et al. 2022).

Cellulose isotope analysis is sometimes preferred over whole wood because it is a very stable compound and avoids the potential issue of variable composition of lignin over the life time of a tree. However, it has also been shown that this may be relevant mostly for long chronologies, but not for short-term ecological studies (Weigt et al. 2015). Often, simply an isotopic offset between resin-extracted wood and cellulose is found, with cellulose having higher $\delta^{13}C$ values by 1-2‰ depending on species (Weigt et al. 2015), which we also observed for the Scots pine samples in our study (Fig. 7). We found that it is possible to do laser ablation on cellulose extracted wood slices, but handling gets more difficult and visibility of rings is reduced which hampers the precise setting of shots. In principle, it might be possible to produce high quality cellulose laths at least for some species (Kagawa et al. 2015). It could also help to prepare holocellulose rather than alpha-cellulose for its higher robustness. Nevertheless, one clear advantage of laser ablation over more conventional techniques, including the splitting of rings or ring sections, is the relatively simple sample preparation, only involving surface preparation. We therefore suggest that cellulose extraction in LA-IRMS studies may only be needed for a selection of samples to determine the offset between the materials, particularly when producing long chronologies. Furthermore, differences between cellulose and wood may be relevant for studying specific questions in carbon allocation, i.e. due to different formation times of cellulose and lignin over the course of the season.

Along with the isotope values, also information about wood density may be retrieved from the mass spectrometer signal, the beam area (Fig. 8). Our results are only preliminary in this respect, because the beam area depends on various settings of the laser and IRMS and should be confirmed by precise analysis of the amount of CO_2, e.g. by Thermal-Conductivity analysis. Furthermore, a careful calibration with conventional methods for determining wood density is necessary (Björklund et al. 2019). However, this option is still very promising. It is well known that LW has a higher density than EW due to smaller cell volumes with thicker cell walls. Wood density also depends on environmental growth conditions. Maximum LW density (MXD) is indeed often measured for climate reconstruction purposes, as it reflects summer temperature particularly in conifers (Schweingruber 1996). This information on wood density is useful on the one hand as a quality control for verifying after the isotope analysis that the shots were placed correctly. In Fig. 8, for instance, it is apparent that the last shot in 2018 was set too close to the edge of the core resulting in a reduced area. As a cautionary note, the dependence of the

460 isotope ratio on the beam area as determined on cellulose materials (see above) is important for
461 correction to avoid any bias on real samples due to wood density fluctuations. On the other
462 hand, this beam area information could ultimately be useful for getting actual wood density data
463 from the laser ablation.

464

465 **4.3 Challenges**

466 Although the previous discussion showed that establishing high-resolution tree-ring isotope
467 data has become relatively straight-forward using LA-IRMS, it should not be neglected that the
468 interpretation of the results remains challenging. Particularly, the relationship between the
469 position of spot on the tree ring with the formation time of this wood is difficult or needs much
470 complementary data on seasonal growth, such as from regular pinning and/or microcore
471 sampling and subsequent wood anatomy (Pérez-de-Lis et al. 2022). An understanding of how
472 the carbon isotope signal is transmitted and recorded in the tree-ring structure is fundamental
473 to soundly interpret isotope data. It is therefore important to consider the development of tree
474 rings over the growing season for relating the tree-ring isotope patterns to seasonal climate data.
475 Tree rings as carbon sinks integrate environmental information over varying time periods
476 depending on the rate to which the cambium forms wood cells and on the longevity of such
477 cells (Cuny et al. 2015). Xylogenesis provides precise information on the timing of cell
478 formation through cambial cell division. Tree-ring anatomy studies can reveal the inter-annual
479 variability of xylem cell number, cell lumen size and cell-wall thickness (von Arx et al. 2016),
480 and provide the spatial context in the ring for timing and duration of wood cell formation and
481 carbon allocation patterns (Martìnez-Sancho et al. 2022). Large, thin-walled EW cells are
482 formed at a high rate, but they only live for days up to a few weeks. Smaller, thick-walled LW
483 cells are built at slow rates, but may live up to several months and integrate environmental
484 information over a much longer period of time (Schollaen et al. 2014). The $\delta^{13}C$ signal in wood
485 depends also on the time lag between sugar production in leaves and wood formation, i.e.
486 translocation of sugars, as well as the use of storage for growth (Gessler and Treydte 2016).
487 These processes all influence the information that can be obtained from a single-shot isotope
488 analysis and therefore the maximal temporal resolution will be restrained rather by the time
489 needed for cell formation than the spatial resolution of the laser. Lignification processes further
490 blur the information between cells as well as the use of carbon from storage (Kagawa et al.
491 2006). Hence, environmental conditions reflected by intra-annual tree-ring parameters are

492 weighted by the seasonal dynamics of wood formation and carbon use (Castagneri et al. 2017;
493 Martìnez-Sancho et al. 2022).

494

495 **4.4 Outlook and conclusions**

496 A systematic assessment and understanding of the climate information in intra-annual $\delta^{13}C$
497 patterns for different species and locations is still missing. In contrast to the numerous annual
498 climate reconstructions, often focusing on average summer climate, only few intra-seasonal
499 reconstructions exist up to date. Such seasonally detailed information is however urgently
500 needed, considering the complex patterns of climate change, which are uneven throughout the
501 year, affecting the seasons differently, and causing pronounced extreme heat waves or heavy
502 precipitation periods, aggravated through the observed increased persistence of pressure
503 systems (Seneviratne et al. 2010; Vogel et al. 2019). There are therefore ample opportunities
504 still for high-resolution research, such as studying narrow tree rings under extreme conditions,
505 like IADFs or "blue rings", which refer to LW cells with reduced or no lignin likely caused by
506 abrupt temperature reduction at the end of the growing season, as were found after volcanic
507 eruptions (Piermattei et al. 2020). A promising field of research also lies in the investigation of
508 carbon dynamics in wood assessed by isotope analysis of carbon storage pools in parenchyma
509 cells.

510 Furthermore, an extension of the system for the analysis of high-resolution tree-ring $\delta^{18}O$ would
511 be desirable. This would further increase the power of the method, in view of many climate
512 studies using a combined $\delta^{13}C$-$\delta^{18}O$-approach and for addressing questions related to tree water
513 sources and hydrology (Büntgen et al. 2021; Saurer and Cherubini 2022). This is in principle
514 possible with the system described, involving a pyrolysis step instead of combustion, followed
515 by conversion of CO to CO_2 by adding one oxygen without changing the isotope ratio of the
516 other (Mak and Yang 1998).

517 The described LA-IRMS system is not only applicable to tree-ring studies, but useful also in
518 other fields where high spatial resolution can provide novel insight into ecological processes.
519 Activity of microbial communities was monitored by LA-IRMS in so-called microbial mats,
520 tightly spaced microbial populations that often show functional stratification (Moran et al.
521 2014). The authors found that it is possible to spatially determine locations within a microbial
522 mat where ^{13}C-labelled substrate accumulates. This could demonstrate where microbial activity
523 is highest and where substrates are consumed within a mat and further show how the activity

changes over diel or seasonal cycles. LA-IRMS might also be applied in animal ecology, particularly by analyzing animal hair at high resolution (Moran et al. 2011). Isotopic analysis of hair samples can provide insights into food sources, seasonal diet variation, or even migration patterns in different animals (Cerling et al. 2006). In van Roij et al. (2017), a technique optimized for small sample amounts was tested where individual pollen grains were analysed for $\delta^{13}C$ by LA-IRMS.

We conclude that high-resolution isotope studies with laser ablation have great promise for exploring many ecological questions in more detail than previously possible, including changes of intrinsic water-use efficiency during the vegetation period. For tree-ring application in climate reconstruction, mostly measured in resin-extracted wood rather than cellulose, there are still major research opportunities, regarding 1) how reliably seasonal/intra-annual climate patterns of the past could be reconstructed at high resolution, 2) what is the influence of species and site conditions, and 3) how do phenological lags and wood formation processes interfere with the aim of deciphering intra-annual climate information.

Funding

We are grateful for support by SNF through instrument funding (206021_189724; R'Equip), project funding (207360) and an Ambizione grant (No. 179978). We also acknowledge funding from ERC (755865) and Academy of Finland (295319).

Acknowledgments

We thank Loïc Schneider and Daniel Nievergelt for their valuable help in sample preparation.

References

Barbour, M.M., A.S. Walcroft and G.D. Farquhar. 2002. Seasonal variation in $\delta^{13}C$ and $\delta^{18}O$ of cellulose from growth rings of Pinus radiata. Plant Cell and Environment. 25:1483-1499.

Battipaglia, G., V. De Micco, W.A. Brand, P. Linke, G. Aronne, M. Saurer and P. Cherubini. 2010. Variations of vessel diameter and $\delta^{13}C$ in false rings of *Arbutus unedo* L. reflect different environmental conditions. New Phytologist. 188:1099-1112.

Belmecheri, S., W.E. Wright, P. Szejner, K.A. Morino and R.K. Monson. 2018. Carbon and oxygen isotope fractionations in tree rings reveal interactions between cambial phenology and seasonal climate. Plant Cell and Environment. 41:2758-2772.

Björklund, J., G. von Arx, D. Nievergelt, R. Wilson, J. Van den Bulcke, B. Gunther, N.J. Loader, M. Rydval, P. Fonti, T. Scharnweber, L. Andreu-Hayles, U. Büntgen, R. D'Arrigo, N. Davi, T. De Mil, J. Esper, H. Gartner, J. Geary, B.E. Gunnarson, C. Hartl, A. Hevia, H. Song, K. Janecka, R.J. Kaczka, A.V. Kirdyanov, M. Kochbeck, Y. Liu, M. Meko, I. Mundo, K. Nicolussi, R. Oelkers, T. Pichler, R. Sanchez-Salguero, L. Schneider, F. Schweingruber, M. Timonen, V. Trouet, J. Van Acker, A. Verstege, R. Villalba, M. Wilmking and D. Frank. 2019. Scientific Merits and Analytical Challenges of Tree-Ring Densitometry. Reviews of Geophysics. 57:1224-1264.

Boettger, T., M. Haupt, K. Knoller, S.M. Weise, J.S. Waterhouse, K.T. Rinne, N.J. Loader, E. Sonninen, H. Jungner, V. Masson-Delmotte, M. Stievenard, M.T. Guillemin, M. Pierre, A. Pazdur, M. Leuenberger, M. Filot, M. Saurer, C.E. Reynolds, G. Helle and G.H. Schleser. 2007. Wood cellulose preparation methods and mass spectrometric analyses of $\delta^{13}C$, $\delta^{18}O$, and nonexchangeable $\delta^{2}H$ values in cellulose, sugar, and starch: An interlaboratory comparison. Analytical Chemistry. 79:4603-4612.

Bose, A.K., A. Rigling, A. Gessler, F. Hagedorn, I. Brunner, L. Feichtinger, C. Bigler, S. Egli, S. Etzold, M.M. Gossner, C. Guidi, M. Levesque, K. Meusburger, M. Peter, M. Saurer, D. Scherrer, P. Schleppi, L. Schonbeck, M.E. Vogel, G. Arx, B. Wermelinger, T. Wohlgemuth, R. Zweifel and M. Schaub. 2022. Lessons learned from a long-term irrigation experiment in a dry Scots pine forest: Impacts on traits and functioning. Ecological Monographs. 92

Büntgen, U., O. Urban, P.J. Krusic, M. Rybnicek, T. Kolar, T. Kyncl, A. Ac, E. Konasova, J. Caslavsky, J. Esper, S. Wagner, M. Saurer, W. Tegel, P. Dobrovolny, P. Cherubini, F. Reinig and M. Trnka. 2021. Recent European drought extremes beyond Common Era background variability. Nature Geoscience. 14:190-+.

Castagneri, D., P. Fonti, G. von Arx and M. Carrer. 2017. How does climate influence xylem morphogenesis over the growing season? Insights from long-term intra-ring anatomy in Picea abies. Annals of Botany. 119:1011-1020.

Cerling, T.E., G. Wittemyer, H.B. Rasmussen, F. Vollrath, C.E. Cerling, T.J. Robinson and I. Douglas-Hamilton. 2006. Stable isotopes in elephant hair document migration patterns and diet changes. Proceedings of the National Academy of Sciences of the United States of America. 103:371-373.

Cuny, H.E., C.B.K. Rathgeber, D. Frank, P. Fonti and M. Fournier. 2014. Kinetics of tracheid development explain conifer tree-ring structure. New Phytologist. 203:1231-1241.

Cuny, H.E., C.B.K. Rathgeber, D. Frank, P. Fonti, H. Makinen, P. Prislan, S. Rossi, E.M. del Castillo, F. Campelo, H. Vavrcik, J.J. Camarero, M.V. Bryukhanova, T. Jyske, J. Gricar, V. Gryc, M. De Luis, J. Vieira, K. Cufar, A.V. Kirdyanov, W. Oberhuber, V. Treml, J.G. Huang, X.X. Li, I. Swidrak, A. Deslauriers, E. Liang, P. Nojd, A. Gruber, C. Nabais, H. Morin, C. Krause, G. King and M. Fournier. 2015. Woody biomass production lags stem-girth increase by over one month in coniferous forests. Nature Plants. 1

Dickmann, D.I. and T.T. Kozlowski. 1970. Mobilization and incorporation of photoassimilated ^{14}C by growing vegetative and reproductive tissues of adult *Pinus resinosa* Ait. trees. Plant Physiology. 45:284-+.

Farquhar, G.D., J.R. Ehleringer and K.T. Hubick. 1989. Carbon isotope discrimination and photosynthesis. Annual Review of Plant Physiology and Plant Molecular Biology. 40:503-537.

598 Fonti, M.V., E.A. Vaganov, C. Wirth, A.V. Shashkin, N.V. Astrakhantseva and E.-D. Schulze. 2018. Age-
599 Effect on Intra-Annual C-13-Variability within Scots Pine Tree-Rings from Central Siberia.
600 Forests. 9
601 Frick, D.A. and D. Günther. 2012. Fundamental studies on the ablation behaviour of carbon in LA-ICP-
602 MS with respect to the suitability as internal standard. Journal of Analytical Atomic
603 Spectrometry. 27:1294-1303.
604 Gärtner, H. and D. Nievergelt. 2010. The core-microtome: A new tool for surface preparation on
605 cores and time series analysis of varying cell parameters. Dendrochronologia. 28:85-92.
606 Gessler, A., J. Pedro Ferrio, R. Hommel, K. Treydte, R.A. Werner and R.K. Monson. 2014. Stable
607 isotopes in tree rings: towards a mechanistic understanding of isotope fractionation and
608 mixing processes from the leaves to the wood. Tree Physiology. 34:796-818.
609 Gessler, A. and K. Treydte. 2016. The fate and age of carbon - insights into the storage and
610 remobilization dynamics in trees. New Phytologist. 209:1338-1340.
611 Ghosh, P. and W.A. Brand. 2004. The effect of N_2O on the isotopic composition of air-CO_2 samples.
612 Rapid Communications in Mass Spectrometry. 18:1830-1838.
613 Hafner, P., J. Gricar, M. Skudnik and T. Levanic. 2015. Variations in Environmental Signals in Tree-Ring
614 Indices in Trees with Different Growth Potential. Plos One. 10
615 Helle, G. and G.H. Schleser. 2004. Beyond CO_2-fixation by Rubisco - an interpretation of $^{13}C/^{12}C$
616 variations in tree rings from novel intra-seasonal studies on broad-leaf trees. Plant Cell and
617 Environment. 27:367-380.
618 Joseph, J., D. Gao, B. Backes, C. Bloch, I. Brunner, G. Gleixner, M. Haeni, H. Hartmann, G. Hoch, C.
619 Hug, A. Kahmen, M.M. Lehmann, M.-H. Li, J. Luster, M. Peter, C. Poll, A. Rigling, K.A.
620 Rissanen, N.K. Ruehr, M. Saurer, M. Schaub, L. Schoenbeck, B. Stern, F.M. Thomas, R.A.
621 Werner, W. Werner, T. Wohlgemuth, F. Hagedorn and A. Gessler. 2020. Rhizosphere activity
622 in an old-growth forest reacts rapidly to changes in soil moisture and shapes whole-tree
623 carbon allocation. Proceedings of the National Academy of Sciences of the United States of
624 America. 117:24885-24892.
625 Kagawa, A., M. Sano, T. Nakatsuka, T. Ikeda and S. Kubo. 2015. An optimized method for stable
626 isotope analysis of tree rings by extracting cellulose directly from cross-sectional laths.
627 Chemical Geology. 393-394:16-25.
628 Kagawa, A., A. Sugimoto and T.C. Maximov. 2006. Seasonal course of translocation, storage and
629 remobilization of C-13 pulse-labeled photoassimilate in naturally growing Larix gmelinii
630 saplings. New Phytologist. 171:793-804.
631 Leavitt, S.W. and A. Long. 1988. Stable carbon isotope chronologies from trees in the Southwestern
632 United States. Global Biogeochemical Cycles. 2:189-198.
633 Loader, N.J., D. McCarroll, S. Barker, R. Jalkanen and H. Grudd. 2017. Inter-annual carbon isotope
634 analysis of tree-rings by laser ablation. Chemical Geology. 466:323-326.
635 Mak, J.E. and W.B. Yang. 1998. Technique for analysis of air samples for C-13 and O-18 in carbon
636 monoxide via continuous-flow isotope ratio mass spectrometry. Analytical Chemistry.
637 70:5159-5161.
638 Martìnez-Sancho, E., K. Treydte, M.M. Lehmann, A. Rigling and P. Fonti. 2022. Drought impacts on
639 tree carbon sequestration and water use - evidence from intra-annual tree-ring
640 characteristics. New Phytologist
641 McCarroll, D. and N.J. Loader. 2004. Stable isotopes in tree rings. Quaternary Science Reviews.
642 23:771-801.
643 Monson, R.K., P. Szejner, S. Belmecheri, K.A. Morino and W.E. Wright. 2018. Finding the seasons in
644 tree ring stable isotope ratios. American Journal of Botany. 105:819-821.
645 Moran, J.J., C.G. Doll, H.C. Bernstein, R.S. Renslow, A.B. Cory, J.R. Hutchison, S.R. Lindemann and J.K.
646 Fredrickson. 2014. Spatially tracking C-13-labelled substrate (bicarbonate) accumulation in
647 microbial communities using laser ablation isotope ratio mass spectrometry. Environmental
648 Microbiology Reports. 6:786-791.

649 Moran, J.J., M.K. Newburn, M.L. Alexander, R.L. Sams, J.F. Kelly and H.W. Kreuzer. 2011. Laser
650 ablation isotope ratio mass spectrometry for enhanced sensitivity and spatial resolution in
651 stable isotope analysis. Rapid Communications in Mass Spectrometry. 25:1282-1290.
652 Nabeshima, E., T. Nakatsuka, A. Kagawa, T. Hiura and R. Funada. 2018. Seasonal changes of δD and
653 δ^{18}O in tree-ring cellulose of *Quercus crispula* suggest a change in post-photosynthetic
654 processes during earlywood growth. Tree Physiology. 38:1829-1840.
655 Nakatsuka, T., M. Sano, Z. Li, C.X. Xu, A. Tsushima, Y. Shigeoka, K. Sho, K. Ohnishi, M. Sakamoto, H.
656 Ozaki, N. Higami, N. Nakao, M. Yokoyama and T. Mitsutani. 2020. A 2600-year summer
657 climate reconstruction in central Japan by integrating tree-ring stable oxygen and hydrogen
658 in isotopes. Climate of the Past. 16:2153-2172.
659 Offermann, C., J.P. Ferrio, J. Holst, R. Grote, R. Siegwolf, Z. Kayler and A. Gessler. 2011. The long way
660 down-are carbon and oxygen isotope signals in the tree ring uncoupled from canopy
661 physiological processes? Tree Physiology. 31:1088-1102.
662 Ogée, J., M.M. Barbour, L. Wingate, D. Bert, A. Bosc, M. Stievenard, C. Lambrot, M. Pierre, T. Bariac,
663 D. Loustau and R.C. Dewar. 2009. A single-substrate model to interpret intra-annual stable
664 isotope signals in tree-ring cellulose. Plant Cell and Environment. 32:1071-1090.
665 Pérez-de-Lis, G., C.B.K. Rathgeber, L. Fernandez-de-Una and S. Ponton. 2022. Cutting tree rings into
666 time slices: how intra-annual dynamics of wood formation help decipher the space-for-time
667 conversion. New Phytologist. 233:1520-1534.
668 Piermattei, A., A. Crivellaro, P.J. Krusic, J. Esper, P. Vitek, C. Oppenheimer, M. Felhofer, N. Gierlinger,
669 F. Reinig, O. Urban, A. Verstege, H. Lobo and U. Büntgen. 2020. A millennium-long 'Blue Ring'
670 chronology from the Spanish Pyrenees reveals severe ephemeral summer cooling after
671 volcanic eruptions. Environmental Research Letters. 15
672 Rinne-Garmston, K.T., G. Helle, M.M. Lehmann, E. Sahlstedt, J. Schleucher and J.S. Waterhouse. 2022.
673 Newer Developments in Tree-Ring Stable Isotope Methods. *In* Stable Isotopes in Tree Rings:
674 Inferring Physiological, Climatic and Environmental Responses Eds. R.T.W. Siegwolf, J.R.
675 Brooks, J. Roden and M. Saurer. Springer International Publishing, Cham, pp 215-249.
676 Rinne, K.T., M. Saurer, A.V. Kirdyanov, N.J. Loader, M.V. Bryukhanova, R.A. Werner and R.T.W.
677 Siegwolf. 2015. The relationship between needle sugar carbon isotope ratios and tree rings
678 of larch in Siberia. Tree Physiology. 35:1192-1205.
679 Rissanen, K., T. Holtta, J. Back, A. Rigling, B. Wermelinger and A. Gessler. 2021. Drought effects on
680 carbon allocation to resin defences and on resin dynamics in old-grown Scots pine.
681 Environmental and Experimental Botany. 185
682 Saurer, M. and P. Cherubini. 2022. Tree physiological responses after biotic and abiotic disturbances
683 revealed by a dual isotope approach. Tree Physiology. 42:1-4.
684 Schollaen, K., H. Baschek, I. Heinrich, F. Slotta, M. Pauly and G. Helle. 2017. A guideline for sample
685 preparation in modern tree-ring stable isotope research. Dendrochronologia. 44:133-145.
686 Schollaen, K., I. Heinrich and G. Helle. 2014. UV-laser-based microscopic dissection of tree rings - a
687 novel sampling tool for δ^{13}C and δ^{18}O studies. New Phytologist. 201:1045-1055.
688 Schulze, B., C. Wirth, P. Linke, W.A. Brand, I. Kuhlmann, V. Horna and E.D. Schulze. 2004. Laser
689 ablation-combustion-GC-IRMS - a new method for online analysis of intra-annual variation of
690 δ^{13}C in tree rings. Tree Physiology. 24:1193-1201.
691 Schweingruber, F.H. 1996. Tree rings and environment—dendrochronology. Haupt, Bern. 609 p.
692 Schweingruber, F.H., H.C. Fritts, O.U. Bräker, L.G. Drew and E. Schär. 1978. The X-ray technique as
693 applied to dendroclimatology. Tree-Ring Bulletin. 38:61-91.
694 Seneviratne, S.I., T. Corti, E.L. Davin, M. Hirschi, E.B. Jaeger, I. Lehner, B. Orlowsky and A.J. Teuling.
695 2010. Investigating soil moisture-climate interactions in a changing climate: A review. Earth-
696 Science Reviews. 99:125-161.
697 Skomarkova, M.V., E.A. Vaganov, M. Mund, A. Knohl, P. Linke, A. Boerner and E.D. Schulze. 2006.
698 Inter-annual and seasonal variability of radial growth, wood density and carbon isotope
699 ratios in tree rings of beech (*Fagus sylvatica*) growing in Germany and Italy. Trees-Structure
700 and Function. 20:571-586.

Szejner, P., W.E. Wright, S. Belmecheri, D. Meko, S.W. Leavitt, J.R. Ehleringer and R.K. Monson. 2018. Disentangling seasonal and interannual legacies from inferred patterns of forest water and carbon cycling using tree-ring stable isotopes. Global Change Biology. 24:5332-5347.

Tang, Y., E. Sahlstedt, G.H.F. Young, P. Schiestl-Aalto, M. Saurer, P. Kolari, T. YJyske, J. Bäck and K.T. Rinne-Garmston. 2022. Intra-seasonal reconstruction of intrinsic water-use efficiency from high-resolution tree ring $\delta^{13}C$ data in boreal Scots pine forests. New Phytologist (under review)

Treydte, K., S. Boda, E.G. Pannatier, P. Fonti, D. Frank, B. Ullrich, M. Saurer, R. Siegwolf, G. Battipaglia, W. Werner and A. Gessler. 2014. Seasonal transfer of oxygen isotopes from precipitation and soil to the tree ring: source water versus needle water enrichment. New Phytologist. 202:772-783.

Treydte, K., D. Frank, J. Esper, L. Andreu, Z. Bednarz, F. Berninger, T. Boettger, C.M. D'Alessandro, N. Etien, M. Filot, M. Grabner, M.T. Guillemin, E. Gutierrez, M. Haupt, G. Helle, E. Hilasvuori, H. Jungner, M. Kalela-Brundin, M. Krapiec, M. Leuenberger, N.J. Loader, V. Masson-Delmotte, A. Pazdur, S. Pawelczyk, M. Pierre, O. Planells, R. Pukiene, C.E. Reynolds-Henne, K.T. Rinne, A. Saracino, M. Saurer, E. Sonninen, M. Stievenard, V.R. Switsur, M. Szczepanek, E. Szychowska-Krapiec, L. Todaro, J.S. Waterhouse, M. Weigl and G.H. Schleser. 2007. Signal strength and climate calibration of a European tree-ring isotope network. Geophysical Research Letters. 34

van Roij, L., A. Sluijs, J.J. Laks and G.J. Reichart. 2017. Stable carbon isotope analyses of nanogram quantities of particulate organic carbon (pollen) with laser ablation nano combustion gas chromatography/isotope ratio mass spectrometry. Rapid Communications in Mass Spectrometry. 31:47-58.

Verheyden, A., G. Helle, G.H. Schleser, F. Dehairs, H. Beeckman and N. Koedam. 2004. Annual cyclicity in high-resolution stable carbon and oxygen isotope ratios in the wood of the mangrove tree Rhizophora mucronata. Plant Cell and Environment. 27:1525-1536.

Vogel, M.M., J. Zscheischler, R. Wartenburger, D. Dee and S.I. Seneviratne. 2019. Concurrent 2018 Hot Extremes Across Northern Hemisphere Due to Human-Induced Climate Change. Earths Future. 7:692-703.

von Arx, G., A. Crivellaro, A.L. Prendin, K. Cufar and M. Carrer. 2016. Quantitative Wood Anatomy-Practical Guidelines. Frontiers in Plant Science. 7

Weigt, R.B., S. Braunlich, L. Zimmermann, M. Saurer, T.E.E. Grams, H.P. Dietrich, R.T.W. Siegwolf and P.S. Nikolova. 2015. Comparison of $\delta^{18}O$ and $\delta^{13}C$ values between tree-ring whole wood and cellulose in five species growing under two different site conditions. Rapid Communications in Mass Spectrometry. 29:2233-2244.

Werner, R.A. and W.A. Brand. 2001. Referencing strategies and techniques in stable isotope ratio analysis. Rapid Communications in Mass Spectrometry. 15:501-519.

Wieser, M.E. and W.A. Brand. 1999. A laser extraction combustion technique for in situ delta C-13 analysis of organic and inorganic materials. Rapid Communications in Mass Spectrometry. 13:1218-1225.

Zalloni, E., G. Battipaglia, P. Cherubini, M. Saurer and V. De Micco. 2018. Contrasting physiological responses to Mediterranean climate variability are revealed by intra-annual density fluctuations in tree rings of Quercus ilex L. and Pinus pinea L. Tree Physiology. 38:1213-1224.

Zhang, H., L. Wei, X. Liao, J.N. Wang, Q.Y. Shi and X. Zhang. 2020. In Situ Carbon Stable Isotope Analysis of Organic Carbon by Laser Ablation-Isotope Ratio Mass Spectrometry. Chinese Journal of Analytical Chemistry. 48:774-779.

749 **Figure caption**

750

751 **Figure 1**

752 Set-up of the LA-IRMS showing the most relevant parts and their connections. After laser
753 ablation (UV laser), the produced gas and particles are lead with helium through a combustion
754 oven and a drying step (Nafion water trap), and the resulting CO_2 is collected in the first trap
755 with LN_2. This trap is then lifted releasing the CO_2 at room temperature. The CO_2 is re-collected
756 in the second, smaller volume trap. During all these steps, the 6-port-valve is in the collection
757 mode (red arrows). The system then switches this valve to the analysis mode (blue arrows), the
758 second trap is lifted and an extra He-supply pushes the sample gas to the GC and the IRMS for
759 analysis.

760 **Figure 2**

761 Sample chamber with two discs of pine saplings (*Pinus sylvestris*) and two reference cellulose
762 pads. Laser shots of 100 µm size are visible in the magnified picture. The yellow inset (optional)
763 is custom-made with a 3D-printer to hold samples in place.

764 **Figure 3**

765 Pfynwald tree-ring sample (tree No. 237) shown for surface prepared with microtome and
766 solvent-extraction (a), additionally polished (b) and after cellulose extraction. Laser marks are
767 visible. Each laser mark is composed of a series of 30 µm spots that are set in parallel to the
768 ring-ring border as a "line of spots". On panel b), laser marks that appear white are the ones
769 from panel a) after polishing.

770 **Figure 4**

771 LA-IRMS results showing $\delta^{13}C$ values of two cellulose standard materials (a), the dependence
772 of $\delta^{13}C$ values on beam area (b) and the dependence of beam area on spot size (c), showing
773 values for single spots as well as line of spots.

774 **Figure 5**

775 Dependence of IRMS intensity (beam area; As = ampere-seconds) on laser power, shown for
776 normal LA-IRMS operating conditions (with combustion) and without combustion.

777 **Figure 6**

LA-IRMS results showing $\delta^{13}C$ values of four Scots pine tree cores, which where $^{13}CO_2$-labeled in late summer 2017 and differently prepared: Blue dots/lines indicate $\delta^{13}C$ values from samples prepared by a microtome before solvent extraction, red dots/lines represent $\delta^{13}C$ values after extraction, and black dots/lines represent $\delta^{13}C$ values after additional polishing. Lighter and darker shades of a colour indicate results from two parallel runs per treatment (see Fig. 3).

Figure 7

LA-IRMS results showing a comparison of Scots pine $\delta^{13}C$ values of wood after extraction (red line/points) with cellulose (black line/points). Lighter and darker shades of a colour indicate results from two parallel runs per treatment.

Figure 8

Beam area of isotope analysis of the Pfynwald tree sample No. 237 from the core prepared with a microtome including solvent extraction (results of two parallel runs on the same core).

Figure 1

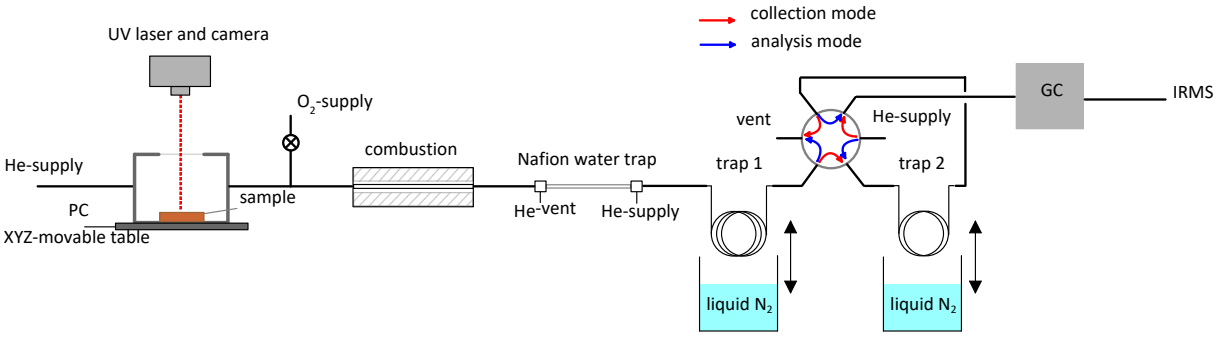
collection mode
analysis mode
UV laser and camera
O_2-supply
He-supply
PC
XYZ-movable table
sample
combustion
Nafion water trap
He-vent
He-supply
vent
He-supply
trap 1
trap 2
GC
IRMS
liquid N_2
liquid N_2

Figure 2

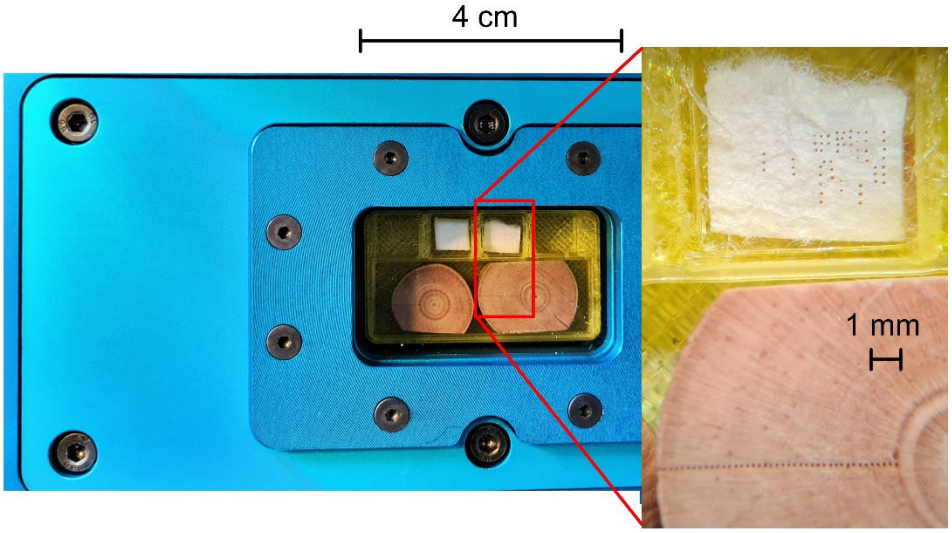

Figure 3

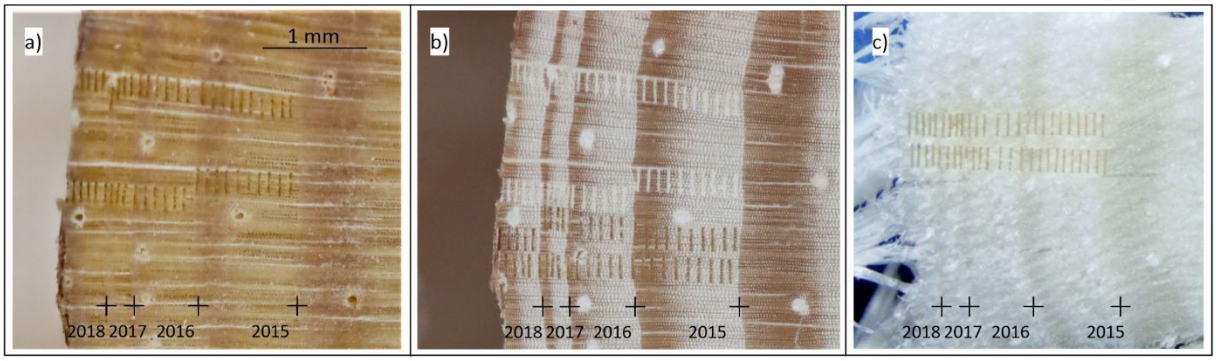
a)
1 mm
2018 2017 2016 2015
b)
2018 2017 2016 2015
c)
2018 2017 2016 2015

Figure 4

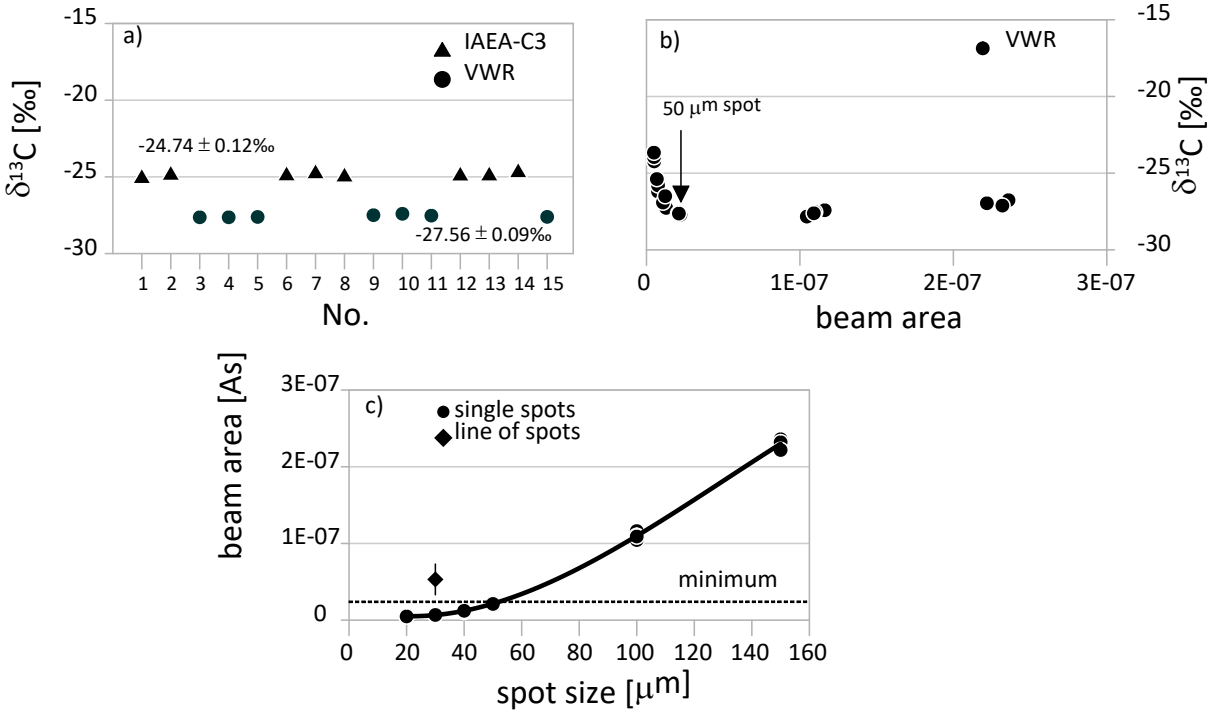
a)
IAEA-C3
VWR
-24.74 ± 0.12‰
-27.56 ± 0.09‰
δ13C [‰]
No.
b)
VWR
50 µm spot
beam area
c)
single spots
line of spots
minimum
beam area [As]
spot size [µm]

Figure 5

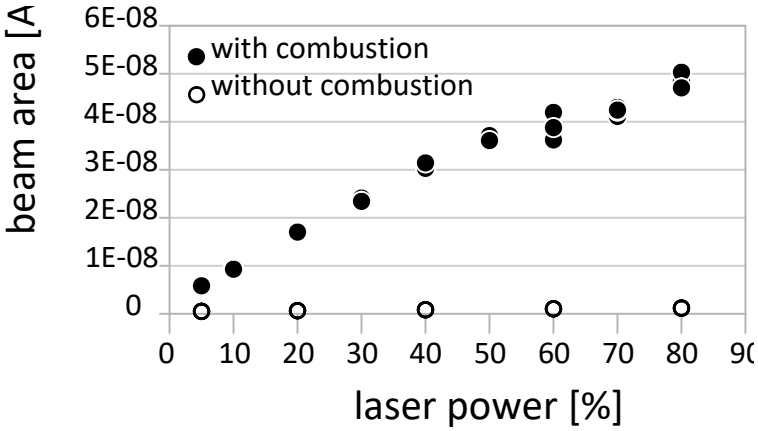
beam area [A
6E-08
5E-08
4E-08
3E-08
2E-08
1E-08
0
with combustion
without combustion
0
10
20
30
40
50
60
70
80
laser power [%]

Figure 6

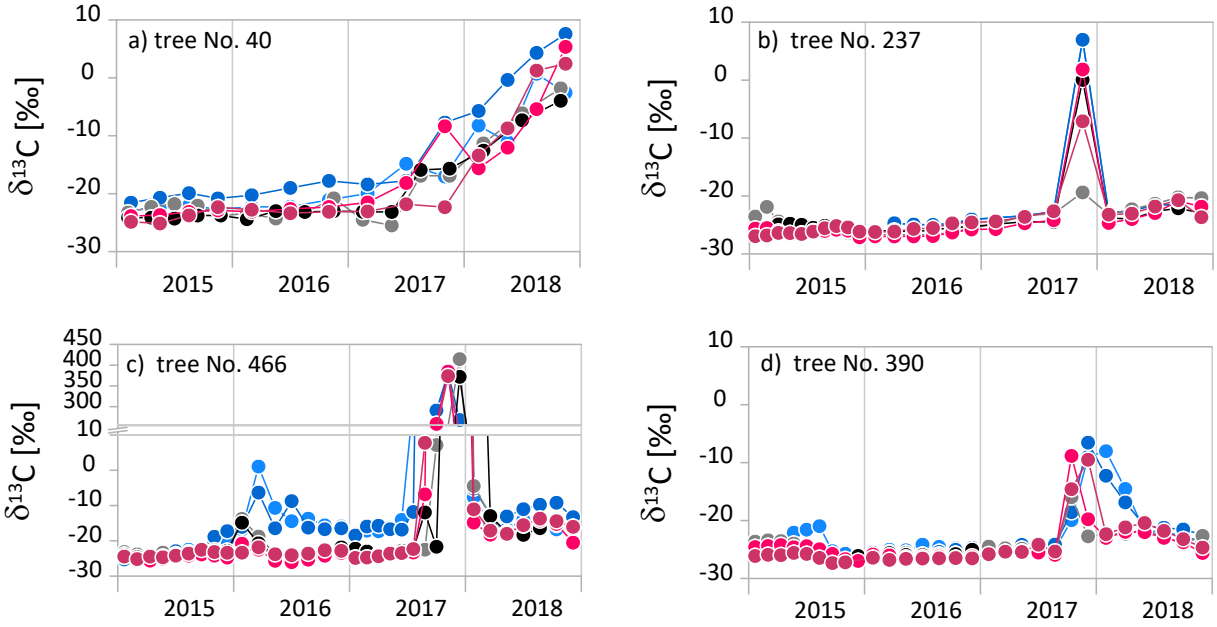
a) tree No. 40
b) tree No. 237
c) tree No. 466
d) tree No. 390
δ13C [‰]
2015
2016
2017
2018

Figure 7

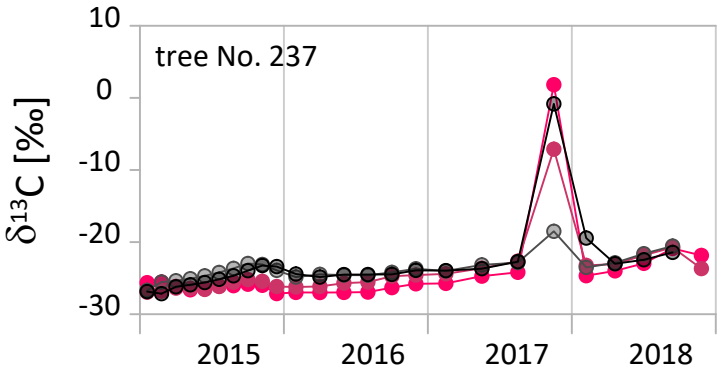

Figure 8

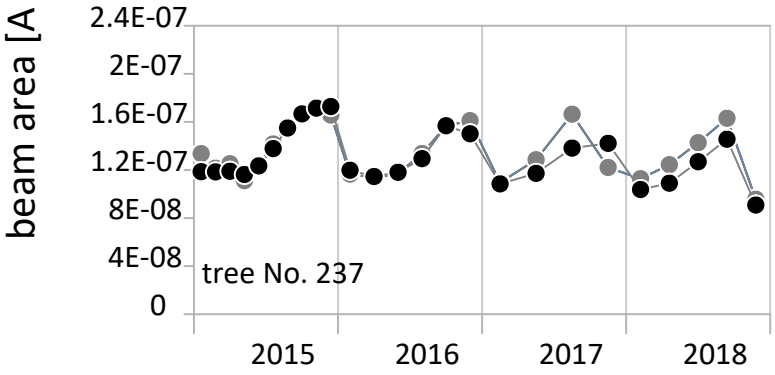
beam area [A
2.4E-07
2E-07
1.6E-07
1.2E-07
8E-08
4E-08
0
tree No. 237
2015
2016
2017
2018